ELSEVIER

Materials Science and Engineering A 435–436 (2006) 132–138

MATERIALS SCIENCE & ENGINEERING A

www.elsevier.com/locate/msea

Formation, thermal stability and deformation behavior of graphite-flakes reinforced Cu-based bulk metallic glass matrix composites

Y.F. Sun [a,*], C.H. Shek [b], S.K. Guan [a], B.C. Wei [c], J.Y. Geng [a]

[a] *Research Center for Materials, Department of Materials Science and Engineering, Zhengzhou University, Zhengzhou 450002, China*
[b] *Department of Physics and Materials Science, City University of Hong Kong, 83 Tat Chee Avenue, Kowloon Tong, Hong Kong, China*
[c] *National Microgravity Lab, Institute of Mechanics, CAS, Beijing 100080, China*

Received 21 June 2006; accepted 14 July 2006

Abstract

Graphite-flake reinforced $Cu_{47}Ti_{34}Zr_{11}Ni_8$ bulk metallic glass matrix composite was fabricated by water-cooled copper mould cast. Most of the graphite flakes still keep unreacted and distribute uniformly in the amorphous matrix except that some reactive wetting occurs by the formation of TiC particles around the flakes. It reveals that the presence of graphite flakes does not affect the onset of the glass transition temperature, crystallization reaction and liquidus of the metallic glass. The resulting material shows obvious serrated flow and higher fracture strength under room temperature compressive load, comparing with the monolithic bulk metallic glass (BMG). Three types of interaction between the shear bands and graphite flakes, namely, shear band termination, shear bands branching and new shear bands formation near the graphite flakes can be observed by quasi-static uniaxial compression test and bonded interface technique through Vickers indentation.

Keywords: Bulk metallic glass; Composites; Mechanical properties

1. Introduction

Bulk metallic glasses (BMGs) have motivated a series of investigations because of their fundamental interest and promising potential for engineering applications. However, in spite of metallic bonding, the lack of dislocations or grain boundary makes the BMGs exhibit shear localization under loading at room temperature, and leads to fracture immediately after yielding of the materials [1–4]. Since BMGs themselves have relatively low melting points and high resistance to heterogeneous nucleation of crystals, considerable effort has been devoted to the development of BMG matrix composites as a way to further improve the mechanical properties compared to monolithic BMGs. It has been shown that BMG reinforced with metal or ceramic particles as well as metal fibers can be successfully processed and the glassy state of the matrix can be retained after processing. The second phase in the glass matrix acts as a 'crack-stopper' by adding impediments to shear band propagation. Therefore, the plastic strain is distributed more homogeneously in the form of shear band patterns, which result in high strains to failure [5–8]. As real hi-tech materials, carbon-fiber and carbon-nanotube have been the latest reinforcement materials used in composites due to their good structural properties, better than those of any metals. For example, Kim et al. [9] reported that carbon-fiber reinforced BMG composites can be prepared successfully by infiltrating liquid Zr–Ti–Cu–Ni–Be into carbon-fiber bundles. Shortly after this, Bian et al. [10–13] synthesized carbon-nanotube reinforced BMG composites, which show excellent wave absorption properties. Comparing with carbon-fiber and carbon-nanotube, graphite flake is a rather common form of carbon but with particular physical and chemical properties. It is widely distributed throughout the world and is one of the softest known materials with a hardness of 1–2 on the Mohs scale. The presence of graphite flakes can exerts a dominant influence on the mechanical properties of the materials. For example, flake-like shape of graphite gives gray cast iron excellent machinability, self-lubricating properties and high damping capacity. In view of these considerations, fabrication of graphite-flake reinforced BMG composites might import some new and useful mechanical properties to the composite.

Up to now, there have been many investigations of the mechanical properties, i.e., deformation, fracture and shear banding, in various BMG alloys and BMG matrix composites

* Corresponding author. Tel.: +86 371 63887506; fax: +86 371 63887508.
E-mail address: yfsun@zzu.edu.cn (Y.F. Sun).

0921-5093/$ – see front matter © 2006 Elsevier B.V. All rights reserved.
doi:10.1016/j.msea.2006.07.040

using the methods of uniaxial compression, tension, bending or nanoindentation, etc. More recently, bonded interface technique through Vickers indentation were used as a very useful method to study the deformed plastic zone beneath an indentation of different kinds of as-cast BMG alloys or as-annealed alloys, which can help image the deformation pattern directly and provides insights into the governing deformation mechanisms [14–17]. In this paper, we report the preparation of graphite-flakes reinforced $Cu_{47}Ti_{34}Zr_{11}Ni_8$ BMG composites. It reveals that the graphite flakes distributed uniformly in the amorphous matrix and the improved mechanical properties were investigated through quasi-static uniaxial compression tests and bonded interface technique through Vickers indentation.

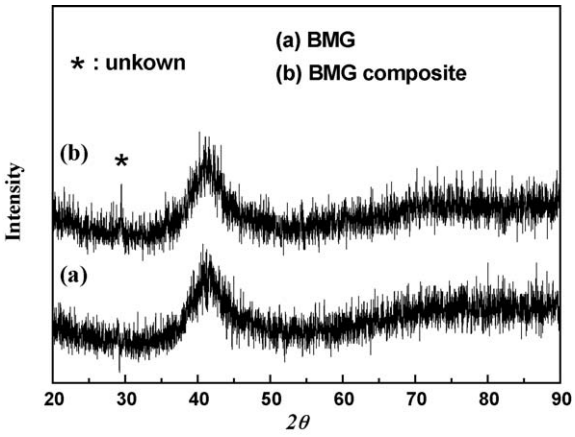

Fig. 1. XRD curves of (a) monolithic BMG and (b) graphite-flake reinforced BMG composite.

2. Experimental procedure

Ingots with a nominal composition of $Cu_{47}Ti_{34}Zr_{11}Ni_8$ were prepared by arc melting a mixture of high purity Zr, Ni, Cu and Ti under a Ti-gettered purified Ar atmosphere. The prepared ingots were broken into small parts and ground mechanically into fine powder with a particle size of about 200 μm. The micron-sized graphite flakes were cleaned in acetone and dehydrated at 373 K. Then the ingot powder was mixed homogeneously with the graphite flakes with volume fraction of 10 vol.%. The mixtures were induction melted under Ar atmosphere and then cast into a water-cooled copper mold to form graphite-flakes reinforced BMG composites with a diameter of 3 mm. For comparison, $Cu_{47}Ti_{34}Zr_{11}Ni_8$ monolithic BMG were also prepared.

The phase constitution of BMG composites were analyzed using a Siemens D500/501 X-ray diffraction (XRD) diffractometer with Cu Kα radiation. The microstructure was observed by using an Axiotech 100 HD optical microscopy and a JEOL 5200 scanning electron microscopy (SEM) equipped with an EDS system. Room temperature compression tests on the cylindrical specimens with an aspect ration of 2:1 were conducted with an Instron 5567 mechanical testing device under quasi-static loading at a strain rate of $1 \times 10^{-4}\,s^{-1}$. Specimens for Vickers indentation were prepared according to the bonded interface technique [19]. Vickers diamond indentations were carried out both on the bonded interface, as well as away from it. Indentations on the interface were carried in such way that one of the indentation diagonals coincided with the interface. Maximum indentation loads applied varied from 500 to 5000 g for the interface indentation as well as for that away from interface. Only those bonded interface specimens were regarded available that the hardness value obtained from indention on the interface were within 10% error comparing to that obtained from indention away from the interface. The bonded interface was subsequently opened by dissolving the adhesive in acetone. Subsurface deformation zones were examined using a JEOL 5200 scanning electron microscopy.

3. Experimental results

3.1. Phase identification and microstructure

Fig. 1 shows the XRD patterns of the monolithic $Cu_{47}Ti_{34}Zr_{11}Ni_8$ BMG and the BMG composite containing graphite flakes. From the curves, each of the sample exhibit a broad diffuse diffraction peak, which is the characteristic of an amorphous structure. No sharp diffraction peaks indicative of the presence of crystalline phase could be detected except a weak crystalline peak with unknown structure for the BMG composite. After introducing graphite flakes into the alloys, it is suggested that small carbon atoms might diffuse into the glass matrix and further increase the complexity of the structure. The amorphous matrix was then stabilized against crystallization.

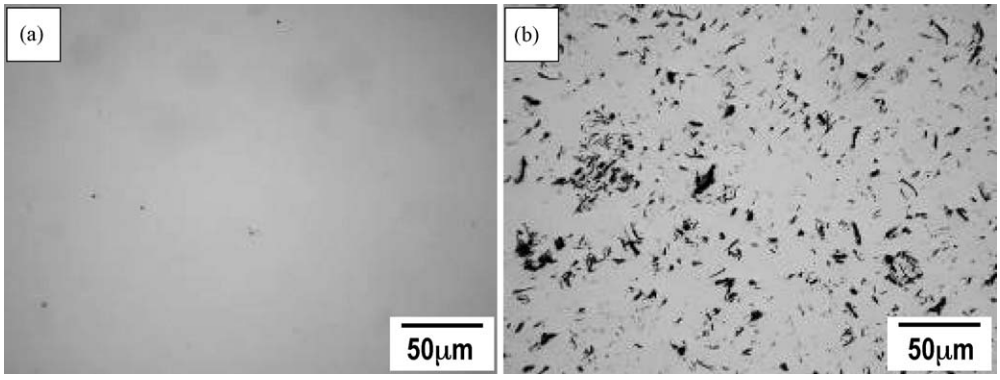

Fig. 2. OM images showing the microstructure of (a) monolithic BMG and (b) graphite-flake reinforced BMG composite.

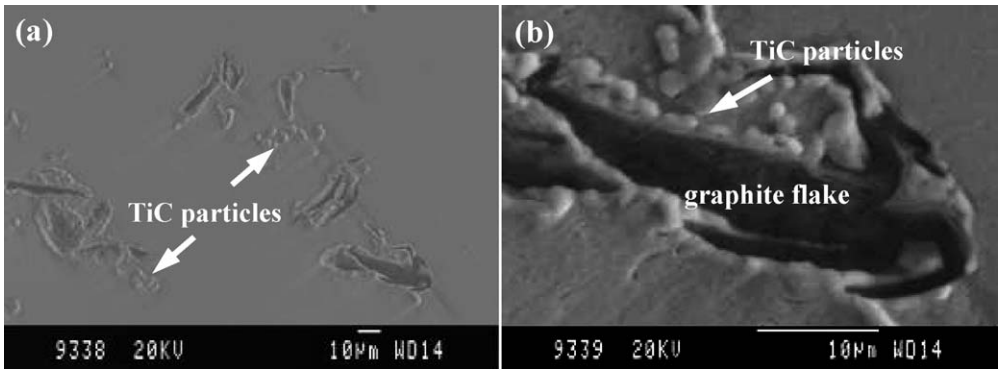

Fig. 3. (a and b) SEM image showing the microstructure of BMG composites containing graphite flakes.

The microstructures of the cross-section of the monolithic $Cu_{47}Ti_{34}Zr_{11}Ni_8$ BMG and the BMG composites containing graphite flakes are shown in Fig. 2. For monolithic BMG, no obvious crystalline precipitates can be found in the homogeneous glass matrix, as shown in Fig. 2(a). For the composites shown in Fig. 2(b), dense black graphite flakes can be found distributed uniformly in the matrix. Neither pores nor voids appear over the whole cross-section of the samples, indicating that a true bonded state exists at the interfaces between the glass matrix and graphite.

To further determine the phase composition of the reinforcement and the matrix, SEM observation as well as electron probe analysis was carried out. Fig. 3(a) shows SEM image of the microstructure of the as-cast graphite-flake reinforced BMG composites. A few polygonal particles with sizes of about 10 μm distributed around the black graphite flakes. However, no such particles can be observed in other regions far from the graphite flakes. Fig. 3(b) shows typical graphite flakes embedded in the glassy matrix at higher magnification. Some spherical particles with an average size of about 2 μm, which are indicated by a white arrow in Fig. 3(b), can be found located in the vicinity of the graphite flakes. Fig. 4(a–c) exhibits the EDS results of the black flakes, the spherical particles and the glass matrix, respectively. The EDS analysis further confirmed that the black phase is graphite flakes. The spherical particles and the polygonal particles have a main composition of Ti and C, and can be identified as TiC phase. The matrix of the composite has a composition of $Cu_{47.1}Ti_{32.3}Zr_{11.8}Ni_{8.8}$, which is very similar to the original composition of the monolithic BMG. However, the content of Ti element is a little lower than that of the original composition due to the reaction with carbon to form TiC phase.

It was well known that the metalloid carbon can form strong covalent bonds with the metallic constituents and cause the formation of easily nucleated crystalline compounds [18,19]. The activation energy of TiC formation was calculated as 731.6 kJ/mol. Warrier et al. considered that the reaction of TiC can occur in two stages: the first stage comprises the formation of TiC layer at the surface of carbon particles and during the second stage, diffusion-controlled growth of TiC occurs. Nucleation of TiC would require the dissolution and rapid diffusion of carbon from the large graphite flakes into the melts, while growth of the carbides would be controlled by the diffusion of the low diffusion species. In some previous work, carbides such as ZrC and TiC were always formed in the Zr-based or Cu-based BMG matrix due to the introduction of carbon solid [12,20]. However, in the present case, although the simultaneous presence of the metallic constituents and the carbon element have a strong

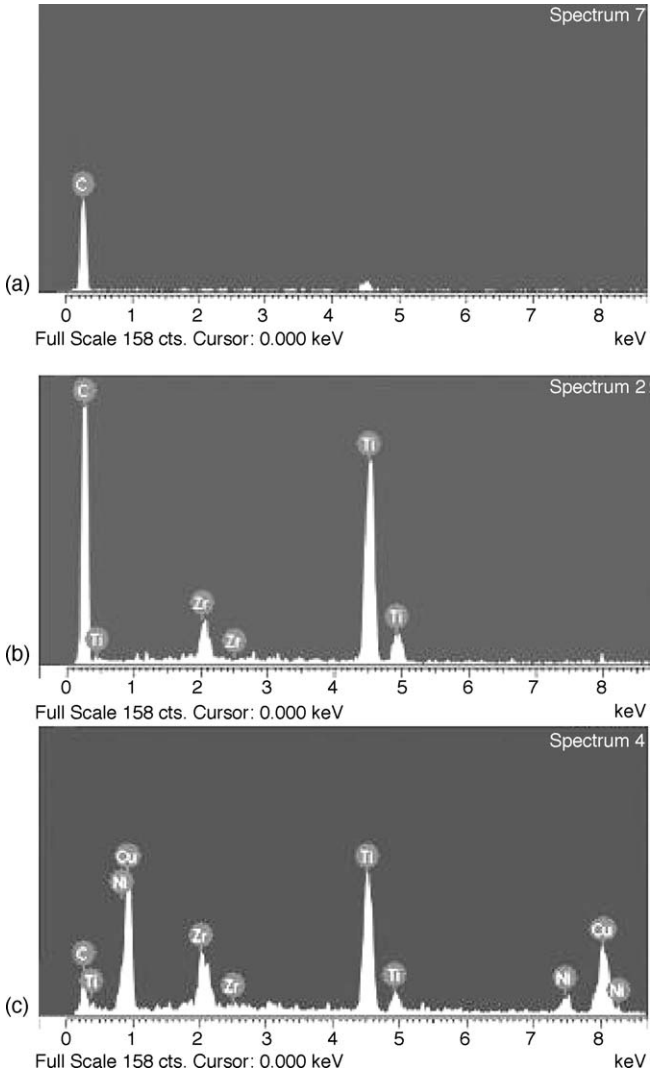

Fig. 4. EDS results corresponds to the different detecting points in Fig. 3.

tendency to form carbide, most part of the graphite flakes still remains unreacted due to the rapid solidification process and lower melting temperature.

3.2. Thermal stability

The high temperature DSC profiles of the two samples are presented in Fig. 5. The DSC curves are very similar at temperatures below 900 K. Each of the DSC curves exhibits an obvious glass transition T_g followed by several exothermic peaks characteristic for stepwise transformations from the supercooled liquid state to the crystalline intermetallic phases. At higher temperature, the DSC curve for monolithic BMG keeps constant until a high endothermal peak corresponding to the onset temperature (T_m) of 1100 K. While for the graphite-flake reinforced BMG composite, the DSC scan dramatically goes downward at 900 K and then gradually goes upward at 990 K. Therefore, a large concavity is formed on the DSC curve before melting occurs, indicating a successively exothermic reaction happens during the heating process. However, the T_g, T_x (crystallization temperature) and T_m are of the same value for the monolithic BMG and the BMG composites. From the above microstructural characterization, the large concavity indicative of successive exothermic reaction on the DSC curve of the BMG composites can be understood. At higher temperature, the diffusion rate of the constitutive element increases greatly and will improve the nucleation and growth of TiC. Therefore, the high temperature DSC curve of the BMG composites in Fig. 5 reveals that the successively exothermic reaction is caused by the formation of TiC phase during the heating process above 900 K.

3.3. Mechanical properties

A series of room temperature compression tests have been carried out for the monolithic $Cu_{47}Ti_{34}Zr_{11}Ni_8$ BMG and the graphite-flakes reinforced BMG composites. Fig. 6 shows the typical compressive stress–strain curves of the two samples. In each case, the sample was tested to failure. For the monolithic BMG, the ultimate compression stress reaches about 2068 MPa,

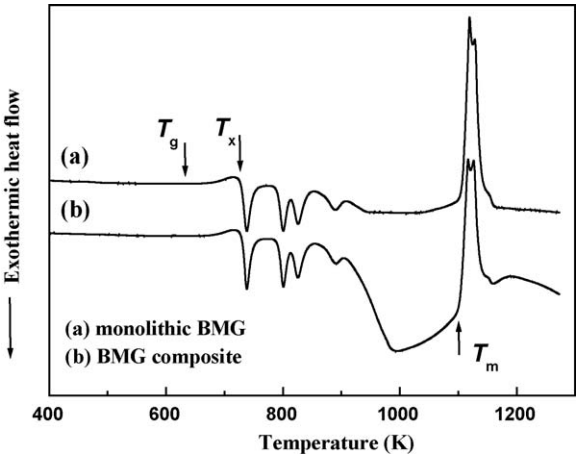

Fig. 5. High temperature DSC curves of (a) monolithic BMG and (b) graphite-flake reinforced BMG composite.

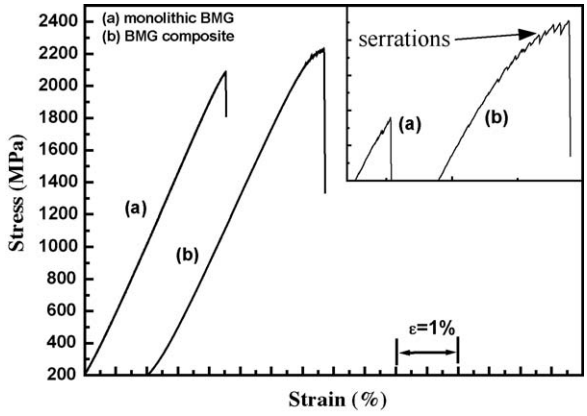

Fig. 6. Room temperature compressive stress–strain curves of (a) monolithic BMG and (b) graphite-flakes reinforced BMG composite.

while that of the BMG composite reaches about 2212 MPa. The monolithic Cu-based BMG does not exhibit any plastic deformation at all. However, it can be seen that the ductility of the graphite flakes contained composite is improved. The plastic elongation after yielding is about 0.5% for the composite. The inset in Fig. 6 exhibits the enlarged serrated flow on the stress–strain curves of the monolithic BMG and the composite, respectively. It reveals that dozens of serrations appear on the stress–strain curve of the composite before failure occurs, while serrations can hardly be found from the stress–strain curves of the monolithic BMG.

It was found that the fractures of the BMG composite containing graphite flakes take place along the maximum shear plane, which is inclined by about 45° to the direction of the applied loading, like that for monolithic BMG. However, fracture morphologies of the two kinds of specimens are markedly different as shown in Fig. 7. The fracture surface of the monolithic BMG (Fig. 7(a)) exhibits vein morphology that is typically seen in the fractographs of metallic glasses, while an interaction between shear bands and the graphite flakes can be found for the BMG composites. Fig. 7(b and c) shows the fracture surface morphology for the BMG composites. Black graphite flake indicated with white arrows can be found lying on the fracture plane. The vein patterns are more complex and branched than that for monolithic BMG. Fig. 7(d) shows the enlarged image of the fracture morphology enclosed in a white square shown in Fig. 7(c). A new vein patterns caused by sweeping through of the shear bands with relatively small width can be seen originating and extending away from the graphite flakes.

To further elucidate the deformation behavior of the BMG composites containing graphite flakes, a bonded interface technique through Vickers indentation was carried out. Fig. 8 shows the top-view of the indentation on the interface of the bonded specimens under a load of 3000 g for the left indentation and 1000 g for the right one. It can be seen that one of the indentation diagonals of each indentation coincides well with the bonded interface. A rather close band is formed between the two halves where the width of the interface is too small and the influence of the adhesive layer can be neglected comparing with the size of the indentation.

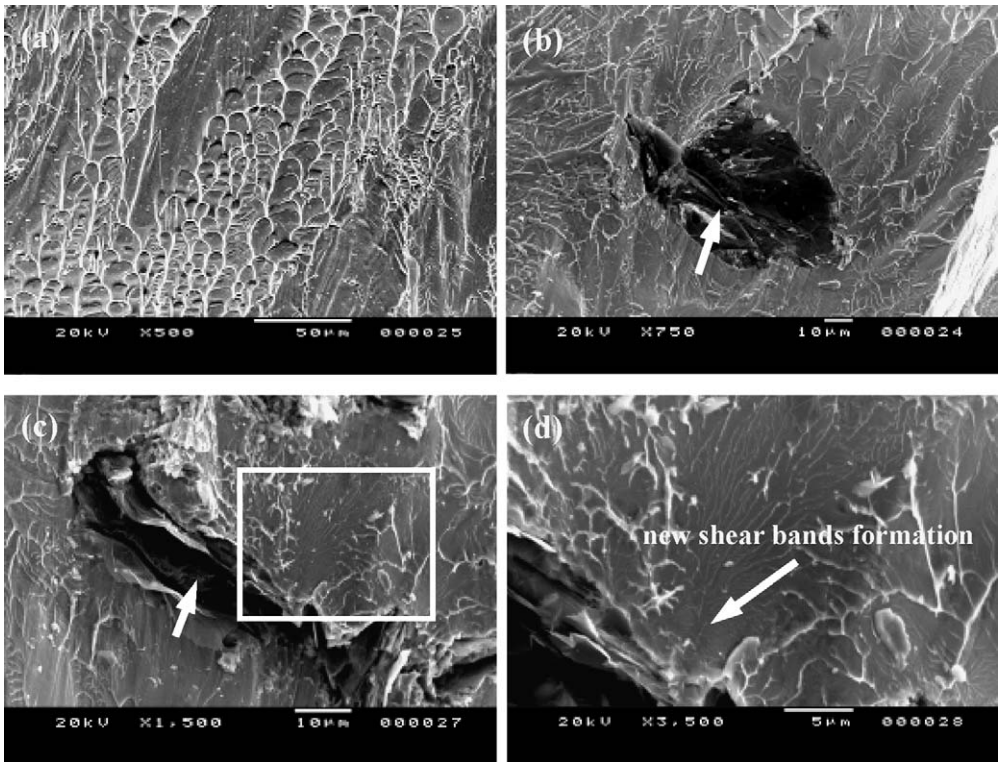

Fig. 7. Fracture surface of the as-cast monolithic BMG and graphite-flakes reinforced BMG composite after compression test: (a) monolithic BMG and (b–d) BMG composites.

After opening carefully the bond, the different deformed morphology for the monolithic BMG and the BMG composites under the indenter tip can be observed readily. Fig. 9(a) shows the typical deformation zone underneath the indention for an applied indentation load of 3000 g for the monolithic BMG. The deformation zone is roughly semi-circular and contains a high density of shear bands. Within the deformation zone shown in Fig. 7(b) at higher magnification, semi-circular and radial shear bands can be seen, which were also found beneath Vickers indentation in other BMG alloy families. There is a very narrow spacing between the adjacent semi-circular shear bands and the spacing increases with the increasing distance of the shear band from the tip of the indenter. Fig. 7(c) shows the morphology of the deformed region underneath an indent for the BMG composites containing graphite flakes. Although the deformed region is still in a semicircle, the shear bands patterns are quite different from that of the monolithic BMG. No radial shear bands but semi-circular ones can be found within the deformed region. Several serrated semi-circular slip-steps due to shear bands are observed. Beyond the serrated slip-steps, numerous smooth slip-steps can also be found between the serrated slip-steps. Due to the presence of the second phase in the glass matrix, the interaction of the shear bands with the graphite flakes occurs. In Fig. 7(d), the termination of shear bands at the graphite flakes can be clearly seen, while in Fig. 7(e), shear bands deviated its direction when meet with the graphite flakes.

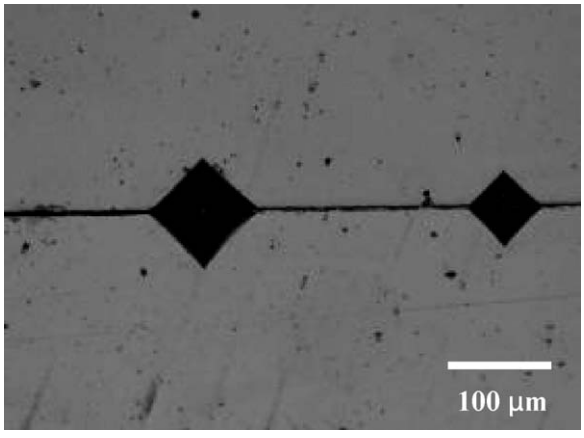

Fig. 8. Representative OM image showing the top-view of indentation impression on the bonded interface.

4. Discussions

In general, bulk single phase amorphous alloys fail due to the formation of shear bands on loading, and this usually results in catastrophic failure. Although one or two kind of fully amorphous bulk metallic alloys have been recently found to exhibit enhanced ductility [21,22], methods for improving the plasticity of bulk amorphous alloys still focus around the addition of a second phase having a different strength and Young's modulus into the glass matrix. This will modify the stress field near the second phase within the amorphous matrix during loading. Therefore, the second phase can serve as an effective barrier to the direct propagation of the shear bands.

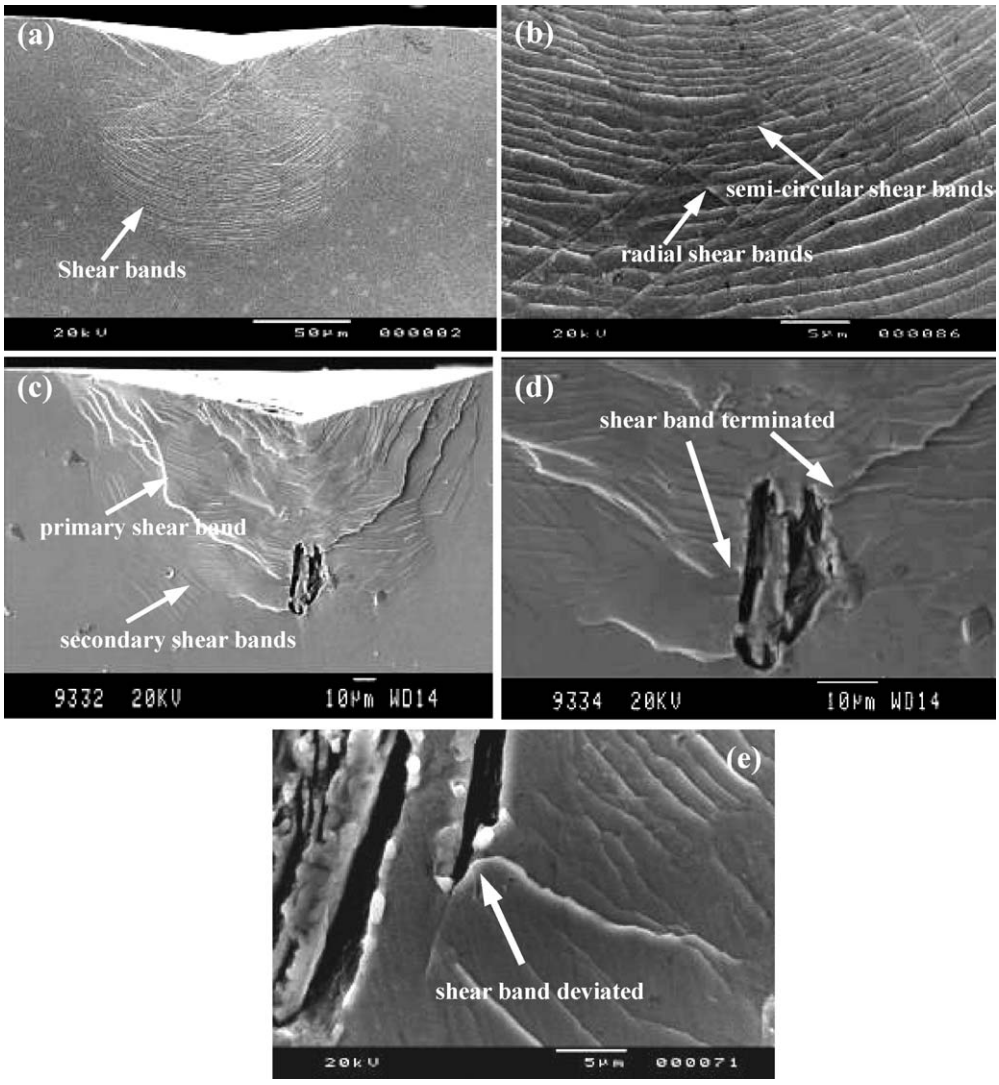

Fig. 9. SEM images showing the subsurface deformation zone underneath a Vickers indentation for (a and b) monolithic $Cu_{47}Ti_{34}Zr_{11}Ni_8$ BMG and (c–e) $Cu_{47}Ti_{34}Zr_{11}Ni_8$ BMG composite containing graphite flakes.

In this investigation, the graphite-flakes reinforced $Cu_{47}Ti_{34}Zr_{11}Ni_8$ BMG composite still fractured by shear band mode. However, it is proposed that the deformation behavior is significantly different from those of other BMG composites. Carbon is found free in nature in three allotropic forms: amorphous, graphite and diamond. Graphite is one of the softest known materials while diamond is one of the hardest. The graphite flakes might act as voids under applied loading in the amorphous matrix due to its very soft property. Improvement of ductility of BMG with honeycomb-like holes has been reported [20]. When the applied stress reaches yield point, shear band nucleate and propagate rapidly along the maximum shear plane. Propagation of shear bands will terminate at the graphite flakes and the nucleation of new shear bands will start to relax the applied stress. Furthermore, the newly nucleated shear band might develop in a different direction and form a branched shear band pattern. The strain will therefore distribute more uniformly in the branched shear bands and avoid the highly localization of shear stress.

On the other hand, the hardness of TiC phase is much higher than that of Cu-based BMG. The formation of TiC particles is also suggested to play an important effect on restricting the shear band propagation and promote the generation of multiple shear bands. Therefore, the presence of TiC particles restrict the slipping of shear bands and make the shear flow more difficult, resulting in increase of compressive fracture strength and ductility. In Fig. 9(e), the deviated shear band is proposed to be caused by the pinning of the hard TiC particles near the graphite flakes. Since the generation of each shear bands refers to single serration on the stress–strain curve, the formation of relatively more shear bands can also be reflected on the stress–strain curves of the samples shown in Fig. 6.

5. Conclusions

(1) $Cu_{47}Ti_{34}Zr_{11}Ni_8$ BMG matrix composite containing uniformly distributed micron-sized graphite flakes can be prepared by Cu mould cast. TiC polygonal or spherical particles

only formed near the graphite flakes. Most of the graphite flakes still keep unreacted due to the rapid solidification process and low melting temperature of the alloy matrix.

(2) The graphite-flake reinforced BMG composite has an improved ultimate fracture strength and obvious ductility comparing with the corresponding monolithic BMG. The fracture strength of the composite reaches 2212 MPa, compared with 2068 MPa of the monolithic BMG. The improved mechanical properties are attributed to the interaction between the graphite flakes and the glass matrix through three methods: shear bands termination, shear bands deviation and new shear bands formation at the graphite flakes.

Acknowledgments

This work was supported by City University of Hong Kong Strategic Research Grant (Project No. 7001529, 7001773) and Nature Science Foundation of China (Grant No. 50571092).

References

[1] A. Inoue, Acta Mater. 48 (2000) 279–306.
[2] A. Peker, W.L. Johnson, Appl. Phys. Lett. 63 (1993) 2342–2344.
[3] H. Bei, Z.P. Lu, E.P. George, Phys. Rev. Lett. 93 (4) (2004) 125504.
[4] A. Inoue, Mater. Trans. JIM 36 (1995) 866–875.
[5] C. Fan, R.T. Ott, T.C. Hufnagel, Appl. Phys. Lett. 81 (2002) 1020–1022.
[6] H. Choi-Yim, W.L. Johnson, Appl. Phys. Lett. 71 (1997) 3808–3810.
[7] R.D. Conner, R.B. Dandliker, W.L. Johnson, Acta Mater. 46 (1998) 6089–6102.
[8] H. Choi-Yim, R. Busch, U. Koster, Acta Mater. 47 (1999) 2455–2462.
[9] C.P. Kim, R. Bush, A. Masuhr, H. Choi-Yim, W.L. Johnson, Appl. Phys. Lett. 79 (1997) 1456–1458.
[10] Z. Bian, R.J. Wang, D.Q. Zhao, Appl. Phys. Lett. 82 (2003) 2790–2792.
[11] Z. Bian, M.X. Pan, Y. Zhang, Appl. Phys. Lett. 81 (2002) 4739–4741.
[12] Z. Bian, R.J. Wang, W.H. Wang, Adv. Funct. Mater. 14 (2004) 55–63.
[13] Z. Bian, R.J. Wang, M.X. Pan, Adv. Mater. 15 (2003) 616–621.
[14] S. Jana, U. Ramamurty, K. Chattopadhyay, et al., Mater. Sci. Eng. A 375–377 (2004) 1191–1195.
[15] H.W. Zhang, X.N. Jing, Subhash Ghatu, et al., Acta Mater. 53 (2005) 3849–3859.
[16] S. Jana, R. Bhowmick, Y. Kawamura, et al., Intermetallics 12 (2004) 1097–1102.
[17] U. Ramamurty, S. Jana, Y. Kawamura, et al., Acta Mater. 53 (2005) 705–717.
[18] S.G. Warrier, R.Y. Lin, Scripta Metall. Mater. 29 (1993) 147–152.
[19] E.L. Zhang, S.Y. Zeng, B. Yang, et al., Metall. Mater. Trans. A 30 (1999) 1147–1162.
[20] H.M. Fu, H.F. Zhang, H. Wang, et al., Scripta Mater. 52 (2005) 669–673.
[21] J. Das, M.B. Tang, K.B. Kim, et al., Phys. Rev. Lett. 94 (4) (2005) 205501.
[22] W.H. Wang, H.Y. Bai, J. Appl. Phys. 84 (1998) 5961–5963.